ACS Catalysis

Research Article

pubs.acs.org/acscatalysis

# L-Proline-Grafted Mesoporous Silica with Alternating Hydrophobic and Hydrophilic Blocks to Promote Direct Asymmetric Aldol and Knoevenagel−Michael Cascade Reactions

Zhe An, Ying Guo, Liwei Zhao, Zhi Li, and Jing He*

State Key Laboratory of Chemical Resource Engineering, Beijing University of Chemical Technology, P.O. Box 98, Beijing 100029, China

Supporting Information

**ABSTRACT:** Promotion of heterogeneous asymmetric catalysis is of major interest in the asymmetric catalysis field. In this work, a novel strategy for the synthesis of L-proline-grafted mesoporous silica with alternating hydrophobic and hydrophilic blocks to promote the heterogeneous asymmetric catalysis was reported. The surface synergies in the neat environment and the interface acceleration in aqueous medium thereby fostered high catalytic activities and enantioselectivity in the direct aldol reaction and the Knoevenagel−Michael cascade reaction. The L-proline loading could be reduced to as low as 0.63 mol %, giving 95% ee for *anti*-isomers and 81% ee for *syn*-isomers in the catalytic asymmetric aldol reaction of nitrobenzaldehyde and cyclohexanone, which was hard to accomplish on the homogeneous counterpart. In the direct asymmetric aldol reaction of ethyl-2-oxoacetate and cyclohexanone, 82% yield in 24 h and 90% ee were achieved. More exciting, the catalysts were applied to more exigent reactions. As an example, in the Knoevenagel−Michael cascade reaction, 85% yield in 10 h and up to 91% ee was achieved.

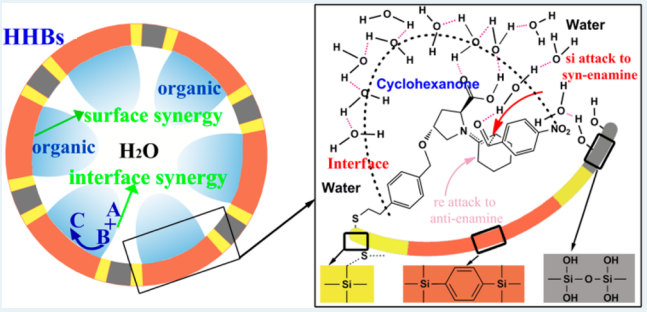


**KEYWORDS:** *asymmetric catalysis, aldol reaction, cascade reaction, surface synergy, interface acceleration, mesoporous silica*

## INTRODUCTION

Improving the catalytic activity and selectivity by virtue of support synergies in the heterogeneous catalysis has always been an important issue.[1−5] However, it remains a challenge especially when it comes to asymmetric reactions.[6−8] Mesoporous silica, with well-ordered nanopores, narrowly distributed pore sizes, and modifiable mesoporous surfaces, provides potential solutions to this issue by demonstrating, for example, confinement effects.[9−13] In metal-catalyzed asymmetric reactions, confining catalytic sites in nanosized channels or pores was observed to visibly improve the catalytic activity and/or enantioselectivity.[14−16] Chiral organocatalysts, which are superior to asymmetric transition-metal catalysts because they are metal-free, inexpensive, stable, and usually capable of working under aerobic atmosphere with wet solvents, have attracted much attention in the past decade.[17,18] Unfortunately, more effective routes or greater success is yet desired for highly efficient and enantioselective heterogeneous organocatalysis.[19,20]

L-Proline was the first reported and one of the most important organocatalysts, demonstrating efficacy in a variety of key asymmetric carbon−carbon and carbon−heteroatom-forming reactions,[21−29] such as Diels−Alder, Michael, Mannich, and especially direct aldol reactions.[30−35] The breakthrough for the asymmetric catalysis of L-proline came from the pioneering work by List and Barbas and their cowokers,[30−32] which applied L-proline as a catalyst for the direct asymmetric aldol reaction between acetone and a variety of aldehydes. Good results were achieved for $\alpha$-branched aliphatic aldehydes; however, quite fair enantioselectivities were observed for aromatic aldehydes. On the other hand, a catalyst loading of as high as 20 to 30 mol % was usually required to obtain a good isolated product yield. Impressive progress has been made in the L-proline-catalyzed direct asymmetric aldol reaction by derivation of proline.[36−41] Using L-proline derivatives, satisfactory enantioselectivity was observed for aromatic aldehydes.[36,37] Implementing L-proline derivative catalyzed asymmetric aldol reactions in water could reduce the catalyst loading from 20 to 30 mol % to less than 10 mol %.[38−43] To derive highly efficient and enantioselective heterogeneous catalyst, attachment of L-proline or its structural analogues to the surfaces of mesoporous silica solids,[44−46] MCM-41, for example, or the interlayer regions of layered solids,[47] layered double hydroxides, for example, was also attempted. Moderate enantiomer excess values were usually achieved. Few positive cases[42,48−54] have been reported recently. But more effective strategies to produce viable

Received: March 24, 2014
Revised: June 19, 2014
Published: June 24, 2014

   dx.doi.org/10.1021/cs500385s | ACS Catal. 2014, 4, 2566−2576

**Scheme 1. Catalysts Prepared in This Work**

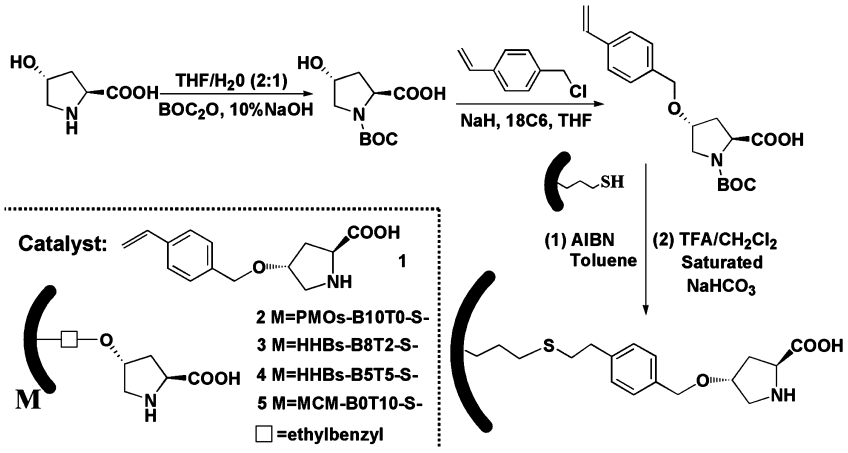


enantioselective heterogeneous catalyst and catalysis in exigent reactions are much in demand.

Here we have demonstrated the achievement of highly efficient and enantioselective catalysis by heterogeneous L-proline catalyst in a quite low loading by use of mesoporous silicas with alternating hydrophobic and hydrophilic blocks (HHBs) in the pore wall. By virtue of the specific microenvironment in the nanochannels of HHBs materials, the resulting heterogeneous catalyst has been found to effectively promote the asymmetric reaction through not only the surface synergy in the neat environment but also the interface acceleration in aqueous medium, which was hard to accomplish with the homogeneous counterpart. In the direct asymmetric aldol reaction of nitrobenzaldehyde and cyclohexanone, 98% yield in 8 h and up to 96% ee were afforded with a proline loading of 6.7 mol %. More exciting, the catalyst could be applied to more exigent reactions with satisfactory yield and enantioselectivity. In the direct asymmetric aldol reaction of ethyl-(2)-oxoacetate and cyclohexanone, 82% yield in 24 h and 90% ee were achieved with a proline loading of 6.3 mol %. In the Knoevenagel–Michael cascade reaction, 85% yield in 10 h and up to 91% ee was achieved with a proline loading of 13.0 mol %.

## EXPERIMENTAL DETAILS

**Preparation of Mercaptopropyl-Functionalized Mesoporous Silicas.** Mercaptopropyl-functionalized mesoporous silicas were synthesized following the method reported by Inagaki et al.[55] with some modifications. Through tailoring the molar ratio of 1,4-bis(triethoxysilyl)benzene (BTEB), tetraethylsilicate (TEOS), and 3-mercaptopropyl-trimethoxysilane (MPTMS), mesoporous with alternating hydrophobic and hydrophilic blocks in the pore wall (HHBs-B8T2-SH, BTEB/TEOS/ MPTMS = 72/18/10; HHBs-B5T5-SH, BTEB/TEOS/MPTMS = 45/45/10), mesoporous silicas with hydrophobic surface (PMOs-B10T0-SH, BTEB/TEOS/MPTMS = 90/0/10), and mesoporous silicas with hydrophilic surface (MCM-B0T10-SH, BTEB/TEOS/ MPTMS = 0/90/10) were prepared. For B*x*T*y*-SH, *x*/*y* represents the molar ratio of BTEB and TEOS, and SH refers to the functionalization with mercaptopropyl group. Typically, cetyltrimethylammonium bromide (CTAB) was dissolved in sodium hydroxide aqueous solution, and then the mixture of BTEB, TEOS, and MPTMS were added to the above solution. The initial molar ratio was set as Si/CTAB/NaOH/$H_2O$ = 1/0.96/2.67/559 for HHBs-B8T2-SH and PMOs-B10T0-SH, and 1/0.96/1.82/559 for HHBs-B5T5-SH. The mixture was treated ultrasonically for 20 min, stirred at room temperature for 12 h, and aged at 90 °C for 24 h. For MCM-B0T10-SH, tetramethylammonium hydroxide Beilstein (TMAH) need to be added,[56] and the initial molar ratio was Si/CTAB/TMAH/NaOH/$H_2O$ = 1/0.27/0.57/0.14/100. The mixture was stirred at room temperature for 1 h and aged at 100 °C for 24 h. The resulting white precipitate was filtrated to yield the as-synthesized sample. CTAB was removed by solvent extraction. As-synthesized sample (1.0 g) was stirred in 200 mL of ethanol with 3.0 g of HCl (36%) at 55 °C for 6 h before filtration.

**Modification of L-Proline.** The following protocol describes the synthesis of *N*-*tert*-butoxycarbonyl-*trans*-4-hydroxy-L-proline: A mixture of *trans*-4-hydroxy-L-proline (1.5 g, 0.038 mol) in a 2:1 mixture of THF/$H_2O$ (75 mL) was treated first with 10% aqueous NaOH (15 mL) and then with di-*tert*-butyldicarbonate (12 g, 0.056 mol). The reaction mixture was stirred at room temperature overnight, and then the THF was removed by vacuum. The residue was adjusted to pH 2–3 by the addition of 10% aqueous $NaHSO_4$. The acidic solution was extracted several times with ethyl acetate. The combined organic extracts were washed with $H_2O$ and brine, and then dried over anhydrous $Na_2SO_4$. Removal of the desiccant and evaporation of the solvent in vacuum gave *N*-*tert*-butoxycarbonyl-*trans*-4-hydroxy-L-proline in a yield of 91%, which was used without further purification. $^1$H NMR (600 MHz, $CDCl_3$): $\delta$ =1.35 (s, 9H, $C(CH_3)_3$), 2.06–2.35 (m, 2H, $\beta$-$CH_2$ Pro), 3.36–3.58 (m, 2H, $\delta$-$CH_2$ Pro), 4.30–4.43 (m, 2H, $\alpha$-CH Pro, $\gamma$-CH Pro). $^{13}$C NMR (400 MHz, $CDCl_3$): $\delta$ = 177.74, 81.99, 77.33, 77.02, 76.70, 54.69, 39.01, 37.3.

The following protocol describes the synthesis of (2*S*,4*R*)-1-(tert-butoxycarbonyl)-4-(4-vinylbenzyloxy)pyrrolidine-2-carboxylic acid: (2*S*,4*R*)-1-(tert-Butoxycarbonyl)-4-(4-vinylbenzyloxy)pyrrolidine-2-carboxylic acid was synthesized following the method reported by Gruttadauria et al.[42,50] with some modifications. A solution of *trans*-Boc-4-hydroxy-L-proline (2.0 g, 8.65 mmol) in anhydrous THF (30 mL) was added dropwise under nitrogen atmosphere to a suspension of NaH (60% mineral oil, 751 mg, 18.77 mmol) in anhydrous THF (20 mL) at 0 °C. The mixture was stirred at ambient temperature for 1 h, and 18-crown-6 (228 mg, 0.86 mmol) and 4-chloromethylstyrene (90%, 2.0 g, 11.6 mmol) were then added. The mixture was stirred for 1 h at ambient temperature and then at 50 °C overnight. After cooling to ambient temperature, water (100 mL) was added. The aqueous phase was extracted with cyclohexane in order to remove the unreacted 4-chloromethylstyrene. The aqueous phase was acidified to pH 2–3 by adding a solution of $NaHSO_4$ (2 M) and was then extracted with ethyl acetate. The organic phase was dried using $MgSO_4$ and concentrated under reduced pressure to give the desired product as pale yellow, viscous oil in 76% yield. $^1$H NMR (600 MHz, $CDCl_3$): $\delta$ = 1.41 (s, 9H, 3x $-CH_3$), 2.10–2.50 (m, 2H, $-CHCH_2CH-$), 3.56–3.62 (m, 2H, $-CHCH_2N-$), 4.14–4.20 (m, 1H, $-OCHH-(CH_2)_2-$), 4.48–4.54 (m, 3H, $-CHCOOH-$ and $-C_6H_4CH_2O-$), 5.25 and 5.75 (2H, HHC=CH), 6.72 (1H, HHC=CH), 7.27 and 7.40 (4H, $-C_6H_4-$). $^{13}$C NMR (400 MHz, $CDCl_3$): $\delta$ = 177.00, 154.30, 137.20, 137.16, 136.38, 127.79, 126.25, 113.87, 80.79, 77.44, 77.32, 76.8, 60.44, 38.84, 37.81.


dx.doi.org/10.1021/cs500385s | ACS Catal. 2014, 4, 2566–2576

**Preparation of L-Proline-Grafted Mesoporous Silica.** The mercaptopropyl-functionalized mesoporous silica (1 g) was added to a degassed solution of (2*S*, 4*R*)-1-(tert-butoxycarbonyl)-4-(4-vinylbenzyloxy)pyrrolidine-2-carboxylic acid (0.52 g, 1.5 mmol) and AIBN (0.024 g, 0.145 mmol) in 50 mL of toluene. The mixture was stirred at 110 °C for 15 h under $N_2$ atmosphere. After cooling to ambient temperature, the solid was filtered and washed with toluene and $CH_2Cl_2$. A light yellow powder was obtained. Finally, the Boc group was removed by suspending the L-proline-grafted solid in 12 mL of $CH_2Cl_2$/TFA (v/v = 3) for 3 h. The solid was filtered and washed with saturated $NaHCO_3$, water, and ethanol. The obtained light yellow powder was dried at 40 °C in vacuum for 24 h.

On the mesoporous support with hydrophobic (PMOs-B10T0-SH), alternating hydrophobic and hydrophilic (HHBs-B8T2-SH and HHBs-B5T5-SH), or hydrophilic (MCM-B0T10-SH) surface, *trans*-4-hydroxy-L-proline was grafted via the covalent linkage using 4-chloromethylstyrene as the linker, producing PMOs-B10T0-Pro (**2**), HHBs-B8T2-Pro (**3**), HHBs-B5T5-Pro (**4**), and MCM-B0T10-Pro (**5**). The preparation of the heterogeneous catalysts was elaborated in Scheme 1. The −OH group passivated HHBs-B8T2-Pro was denoted as HHBs-B8T2-Pro-$CH_3$ (**3′**).

**Characterization.** Powder X-ray diffraction patterns were obtained on a Bruker D8 focus X-ray diffractometer with Cu K$\alpha$ radiation operated at 30 mA and 45 kV. TEM images were taken on a JEOL JEM-2010 electron microscope operating at 200 kV. Nitrogen adsorption/desorption experiments were performed at 77 K on a Quantachrome Autosorb-1 system. The samples were degassed at 80 °C for 5 h prior to measurements. The specific surface area was calculated by the standard BET method. The mesopore size distribution was calculated from the desorption branch using the Barret-Joyner-Halenda (BJH) method. The microporous surface area and volume were calculated using the t-plot method. The external surface area was calculated using the high-resolution $\alpha_s$-plot method.[57] FT-IR spectra were recorded using a Nicolet 380 (Thermo) spectrophotometer in the range of 4000−300 $cm^{-1}$ with 1 $cm^{-1}$ resolution with the pristine sample pellets treated in vacuum for 6 h. Thermogravimetric analysis and differential thermal analysis (TG-DTA) were carried out on a Pyris Diamond TG/DTA thermal analysis system by PerkinElmer Instrument. HPLC was carried out using Varian Prostar 210 HPLC with Prostar 325 UV−vis detector. $^1$H NMR spectra of the liquid compounds were recorded on a Bruker Avance-400 spectrometer running at 400 MHz (Bruker, Bremen, Germany), in $CDCl_3$ as the solvent. Chemical shifts were reported in the $\delta$ scale relative to residual $CHCl_3$ (7.26 ppm) for $^1$H NMR. Data for $^1$H NMR are recorded as follows: chemical shift ($\delta$, ppm), multiplicity (s, singlet; d, doublet; t, triplet; q, quartet; m, multiplet), intergration, coupling constant (Hz). The solid-state NMR experiments were carried out at 59.6 and 75.5 MHz for $^{29}$Si and $^{13}$C, respectively, on a Bruker Avance-400 M solid-state spectrometer equipped with a commercial 4 mm MAS NMR probe. The chemical shifts were determined using $\delta_{TMS}$ = 0 ppm as a reference. The magic-angle spinning frequencies were set to 5 kHz for all experiments. $^{29}$Si BD/MAS NMR spectra for the silanol determination were carried out using an Hpdec pulse sequence, which is one pulse sequence with a high power proton decoupling. Mass spectra were recorded on a micromass LCT spectrometer using electrspray ($ES^+$) ionization techniques.

**General Procedure for Aldol Reactions.** Typically, 83 $\mu$L of cyclohexanone was added to 12 mg catalyst in a microreaction flask. The proline loading was 10% for (2*S*, 4*R*)-1-(*tert*-butoxycarbonyl)-4-(4-vinylbenzyloxy) pyrrolidine-2-carboxylic acid, 8.2% for PMOs-B10T0-Pro, 6.7% for HHBs-B8T2-Pro, 5.9% for HHBs-B5T5-Pro, and 5.5% for MCM-B0T10-Pro. After sufficient wetting, 331 $\mu$L of water was added. Stirred for 5 min, 7.6 mg (0.05 mmol) of *p*-nitrobenzaldehyde was added. The reaction mixture was stirred at 25 °C for 24 h, extracted with ethyl acetate (3 × 1 mL). The resulting organic extracts were dried using $Na_2SO_4$. After removal of the catalyst by filtration, diastereoselectivity and conversion were determined by $^1$H NMR analysis of the crude aldol product. Purification by flash column chromatography (silica gel, hexane/AcOEt) gave the aldol product as a colorless solid. The enantiomeric excess of product was determined by chiral-phase HPLC analysis (column: Chiralpak AD-H; flow phase: isopropanol/*n*-hexane (v/v = 5/95); flow rate: 1.0 mL/min; detection wavelength: 254 nm). The absolute configuration of aldol products was determined according to refs 39 and 58. The product analysis by NMR and HPLC are elaborated in the Supporting Information.

*General Procedure for Knoevenagel−Michael Cascade Reaction.* Typically, 0.5 mmol of isatin, 0.5 mmol of malononitrile, 0.5 mmol of acetone, 5 mL of solvent, and 240 mg of catalyst were oscillated at room temperature for 10 h. The reaction progress was monitored by TLC (hexane/ethyl acetate (v/v = 7/3)). The proline loading was 20.0% for (2*S*, 4*R*)-1-(*tert*-butoxycarbonyl)-4-(4-vinylbenzyloxy) pyrrolidine-2-carboxylic acid, 15.0% for PMOs-B10T0-Pro, 13.0% for HHBs-B8T2-Pro, 12.0% for HHBs-B5T5-Pro, and 11.2% for MCM-B0T10-Pro. The resulting organic extracts were dried using $Na_2SO_4$. After removal of catalyst by filtration, conversion was determined by $^1$H NMR analysis of the crude product. Purification by flash column chromatography (silica gel, hexane/AcOEt) gave the product as a red solid. The enantiomeric excess of product was determined by chiral-phase HPLC analysis (column: Chiralpak AD-H; flow phase: isopropanol/*n*-hexane (v/v = 30/70); flow rate: 1.0 mL/min; detection wavelength: 254 nm). The absolute configuration of the products was determined according to ref 59. Product analysis by NMR and HPLC are elaborated in the Supporting Information.

**Catalyst Recycling.** The catalyst was recycled easily from the reaction system by centrifugation. The resulting solid was thoroughly rinsed with ethyl acetate, deionized water, and ethanol for 5 times separately and dried in vacuum at 40 °C for the recycling catalytic experiments.

## RESULTS AND DISCUSSION

**Structural Properties of Heterogeneous L-Proline Grafted Mesoporous Silica Catalyst.** The powder X-ray diffraction pattern of HHBs-B8T2-SH (Figure 1a) shows

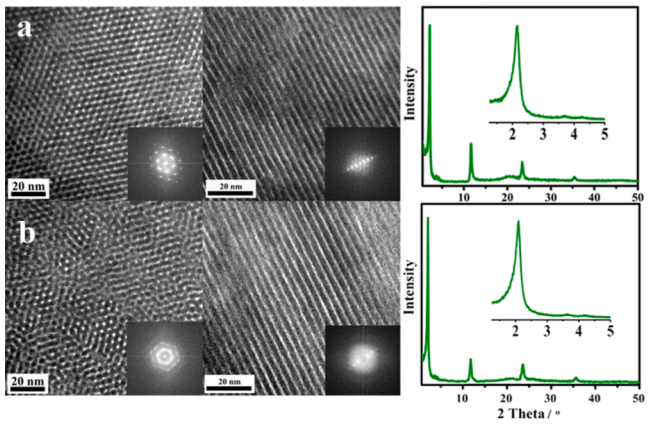


**Figure 1.** TEM images (inset: electron diffraction patterns) and wide and low (inset) angle powder XRD patterns of (a) HHBs-B8T2-SH and (b) HHBs-B8T2-Pro.

typical 100, 110, and 200 reflections with a spacing of 41.0, 23.7, and 20.8 Å in the low-angle diffraction region ($2\theta$<10°), which can be assigned to the two-dimensional hexagonal symmetry (*p6mm*) lattice. The peaks at *d* spacing of 7.6, 3.8, and 2.5 Å in the region 10° < $2\theta$ < 50° can be assigned to a periodic structure[55,60] with a spacing of 7.6 Å existing in the pore walls. The well-ordered hexagonally symmetric structures are fully confirmed by the TEM images. As a comparison, well-defined hexagonally symmetric mesoporous structures can be also observed from XRD patterns (Figure S1A) and TEM images (Figure S2, upper images) for PMOs-B10T0-SH,


dx.doi.org/10.1021/cs500385s | ACS Catal. 2014, 4, 2566−2576

**Table 1. Textural Parameters of the Mercaptopropyl-Functionalized Samples and the L-Proline Grafted Catalysts**

| sample | $S_{BET}$ ($m^2/g$) | $S_{micro}$ ($m^2/g$) | $S_{meso}$ ($m^2/g$) | $S_{ex}$ ($m^2/g$) | pore volume ($cm^3/g$) | $V_{micro}$ ($cm^3/g$) | $V_{meso}$ ($cm^3/g$) | pore size[a] (nm) | wall thickness[b] (nm) |
|---|---|---|---|---|---|---|---|---|---|
| PMOs-B10T0-SH | 1330 | 0 | 1310 | 20 | 0.95 | 0 | 0.95 | 2.46 | 1.05 |
| PMOs-B10T0-Pro | 1303 | 6 | 1280 | 17 | 0.91 | 0.03 | 0.88 | 2.44 | 1.10 |
| PHHBs-B8T2-SH | 1506 | 0 | 1482 | 24 | 1.12 | 0 | 1.12 | 2.45 | 1.10 |
| PHHBs-B8T2-Pro | 1486 | 0 | 1465 | 21 | 1.07 | 0 | 1.07 | 2.43 | 1.16 |
| PHHBs-B5T5-SH | 1239 | 3 | 1205 | 31 | 1.05 | 0.02 | 1.03 | 2.49 | 1.11 |
| PHHBs-B5T5-Pro | 875 | 0 | 858 | 17 | 0.86 | 0 | 0.86 | 2.50 | 1.19 |
| MCM-B0T10-SH | 1257 | 0 | 1221 | 36 | 0.95 | 0 | 0.95 | 2.44 | 1.18 |
| MCM-B0T10-Pro | 817 | 0 | 801 | 16 | 0.58 | 0 | 0.58 | 2.42 | 1.25 |

[a]Pore size at the maximum distribution. [b]Estimated as the difference between the parameter *a* from XRD patterns and the pore size from $N_2$ sorption.

HHBs-B5T5-SH, and MCM-B0T10-SH. The periodic structures existing in the pore walls are also clearly observed for PMOs-B10T0-SH and HHBs-B5T5-SH. All the mercaptopropyl-functionalized samples exhibit typical type IV nitrogen adsorption−desorption isotherms, with a uniform pore size distribution at a maximum of 2.46−2.50 nm (Figure S3A). The detailed textural parameters have been illustrated in Table 1. Almost no micropores exist in the mercaptopropyl-functionalized samples.

Solid-state $^{29}Si$ and $^{13}C$ NMR spectroscopies have been demonstrated to be the most useful for providing chemical information regarding the condensation of organosiloxane and siloxane. As shown in the $^{29}Si$ BD/MAS NMR spectra (Figure 2), HHBs-B8T2-SH, HHBs-B5T5-SH, and MCM-B0T10-SH materials demonstrate two sets of broad signals attributed to the resonances for organosiloxane ($T_m$ = $RSi(OSi)_m(OH)_{3-m}$, $m$ =1−3, −50 to −80 ppm) and for siloxane ($Q_n$ = $Si(OSi)_n(OH)_{4-n}$, $n$ = 2−4, −90 to −120 ppm) environments. There is no Q linkage observed for PMOs-B10T0-SH. The presence of the $T_m$ units gives evidence of the existence of C−Si covalent bonds. The silanol density was quantified by curve fitting and deconvolution of $^{29}Si$ BD/MAS NMR signals according to the reference method.[61] The calculated formula is exhibited as follows:

$$\text{silanol density } (\mu\text{mol}\cdot\text{g}^{-1}) = \sum W_{Q_n}\cdot M_{Q_n} + \sum W_{T_m}\cdot M_{T_m}$$

wherein $W$ and $M$, respectively, represent the peak area percentage and the molar mass of $Q_n$ and $T_m$ ($n$ = 2−4; $m$ = 1−3). Silanol density was calculated as 4.23, 4.78, 5.12, and 7.19 mmol/g for PMOs-B10T0-SH, HHBs-B8T2-SH, HHBs-B5T5-SH, and MCM-B0T10-SH, as shown in Table 2. The vacuum FT-IR spectra (Figure S4) also clearly show the stronger Si−OH band of MCM-B0T10-SH than that of HHBs-B8T2-SH, confirming the more silanol quantity for MCM-B0T10-SH than HHBs-B8T2-SH. In the $^{13}C$ CP/MAS NMR spectra for PMOs-B10T0-SH, HHBs-B8T2-SH, and HHBs-B5T5-SH (Figure S5a, 5c, 5e), the occurrence of a large peak at about 134.7 ppm along with sidebands (denoted with asterisks) is attributed to the phenylene group connected to Si.[62] For MCM-B0T10-SH (Figure 3A), the resonance at 25.3 ppm could be assigned to the $^3CH_2$ attached to the SH moieties,[63] whereas the resonances of the $^1CH_2$ and $^2CH_2$ carbons appear at 4.6 and 46.2 ppm, respectively. No resonance for the $^3CH_2$ attached to the $-SO_3H$ moieties was detected, excluding the possibility of the transformation from thiol to sulfonic groups by the acid extraction.

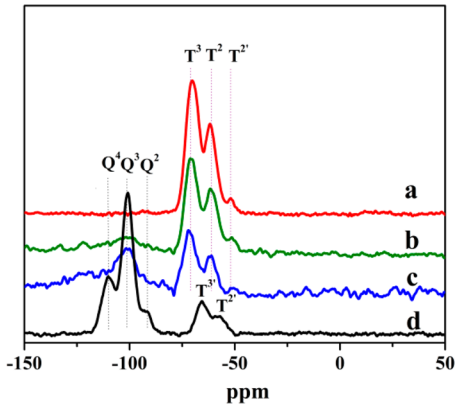


**Figure 2.** $^{29}Si$ BD/MAS NMR spectra of (a) PMOs-B10T0-SH, (b) HHBs-B8T2-SH, (c) HHBs-B5T5-SH, and (d) MCM-B0T10-SH.

**Table 2. Surface Properties and Chemical Composition of the Mercaptopropyl-Functionalized Samples and the L-Proline-Grafted Catalysts**

| samples | S content (mmol/g) | −OH[a] (mmol/g) | phenyl/OH (mol/mol) | $C_{BET}$[b] | N content (mmol/g) |
|---|---|---|---|---|---|
| PMOs-B10T0-SH | 0.43 | 4.23 | 1.18 | 0.83 | 0 |
| PMOs-B10T0-Pro | 0.43 | | | 0.65 | 0.34 |
| HHBs-B8T2-SH | 0.44 | 4.78 | 1.02 | 1.34 | 0 |
| HHBs-B8T2-Pro | 0.43 | | | 1.24 | 0.28 |
| HHBs-B5T5-SH | 0.42 | 5.12 | 0.65 | 2.21 | 0 |
| HHBs-B5T5-Pro | 0.42 | | | 2.07 | 0.25 |
| MCM-B0T10-SH | 0.40 | 7.19 | 0 | 5.07 | 0 |
| MCM-B0T10-Pro | 0.40 | | | 4.88 | 0.23 |

[a]−OH content was calculated from $^{29}Si$ BD/MAS NMR spectra; [b]$C_{BET}$ parameter was calculated from the vapor adsorption isotherm by the BET method.


dx.doi.org/10.1021/cs500385s | ACS Catal. 2014, 4, 2566−2576

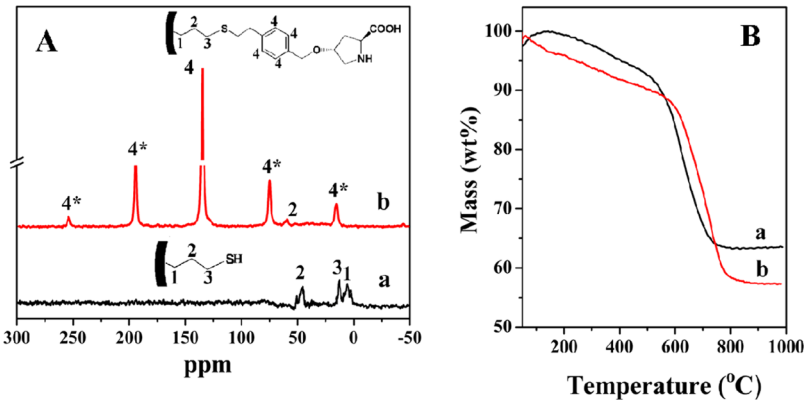


**Figure 3.** (A) $^{13}C$ CP/MAS NMR spectra of (a) MCM-B0T10-SH and (b) MCM-B0T10-Pro (* refers to sidebands). (B) TGA curves of (a) HHBs-B8T2-SH and (b) HHBs-B8T2-Pro.

**Table 3. Direct Asymmetric Aldol Reaction of Cyclohexanone with Aldehydes in Neat or Medium[a]**

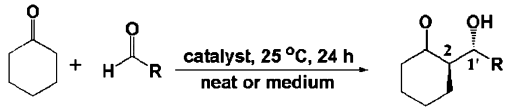


| | | | | | | | | | ee (%)[b] | |
|---|---|---|---|---|---|---|---|---|---|---|
| entry | R = | cat. | proline loading (mol %) | time (h) | solvent | yield (%) | TON | *anti*/*syn*[b] | *anti* | *syn* |
| 1[c,f] | *p*-nitrobenz- | 1 | 10 | 72 | | <3 | | | | |
| 2[c,f] | | 2 | 8.2 | 24 | | 58 | 7.0 | 76:24 | 73 | 57 |
| 3[c,f] | | 3 | 6.7 | 24 | | 42 | 6.4 | 79:21 | 89 | 78 |
| 4[c,f] | | 4 | 5.9 | 24 | | 27 | 3.3 | 76:24 | 80 | 60 |
| 5[c,d,f] | | 5 | 5.5 | 48 | | <3 | | | | |
| 6[c,f] | | 3′ | 6.7 | 24 | | 41 | 6.0 | 76:24 | 78 | 56 |
| 7 | | 1 | 10 | 72 | $H_2O$ | <3 | | | | |
| 8[f] | | 2 | 8.2 | 24 | $H_2O$ | 96 | 11.7 | 86:14 | 22 | 14 |
| 9[f] | | 3 | 6.7 | 24 | $H_2O$ | 83 | 12.6 | 87:13 | 72 | 28 |
| 10 | | 3 | 6.7 | 48 | $H_2O$ | 98 | 14.9 | 87:13 | 72 | 38 |
| 11[f] | | 4 | 5.9 | 24 | $H_2O$ | 48 | 5.7 | 84:16 | 74 | 18 |
| 12[f] | | 5 | 5.5 | 24 | $H_2O$ | 18 | 3.7 | 78:22 | 25 | 6 |
| 13 | | 1 | 10 | 72 | brine | <3 | | | | |
| 14 | | 2 | 8.2 | 8 | brine | 62 | 7.5 | 88:12 | 83 | 62 |
| 15[f] | | 2 | 8.2 | 24 | brine | >99 | 12.0 | 86:14 | 72 | 39 |
| 16[f] | | 3 | 6.7 | 8 | brine | 98 | 14.9 | 90:10 | 96 | 85 |
| 17[f] | | 3 | 6.7 | 24 | brine | >99 | 15.1 | 90:10 | 96 | 84 |
| 18 | | 4 | 5.9 | 24 | brine | 31 | 3.7 | 91:9 | 84 | 41 |
| 19 | | 5 | 5.5 | 24 | brine | 24 | 5.0 | 77:23 | 33 | 17 |
| 20[d,f] | | 3 | 0.63 | 24 | brine | 54 | 81.8 | 90:10 | 95 | 81 |
| 21[f] | | 3′ | 6.7 | 8 | brine | 85 | 11.3 | 89:21 | 80 | 20 |
| 22[f] | | 2 | 8.0 | 8 | toluene | 27 | 2.1 | 71:29 | 60 | 26 |
| 23[f] | | 3 | 6.7 | 8 | toluene | 21 | 2.1 | 80:20 | 49 | 5 |
| 24[e,f] | | 3 | 6.7 | 8 | toluene/brine | 28 | 2.5 | 81:19 | 69 | 7 |
| 25 | | 3 | 6.7 | 8 | DMSO | 33 | 4.7 | 78:22 | 79 | 28 |
| 26 | *m*-nitrobenz- | 3 | 6.7 | 48 | brine | 93 | 13.8 | 84:16 | 75 | 36 |
| 27 | *o*-nitrobenz- | 3 | 6.7 | 48 | brine | 78 | 11.6 | 66:34 | 92 | 15 |
| 28 | -$CO_2$Et | 3 | 6.3 | 24 | brine | 81 | 13.0 | 80:20 | 90 | n.d.[g] |

[a]Conditions: aldehyde (0.05 mmol), cyclohexanone (83 μL, 0.8 mmol), and solvent (331 μL). [b]Determined by $^1H$ NMR of the crude product and chiral-phase HPLC analysis. [c]The reaction in neat cyclohexanone (414 μL). [d]Conditions: *p*-nitrobenzaldehyde (0.53 mmol), cyclohexanone (83 μL, 0.8 mmol), and saturated brine (331 μL). [e]Toluene/brine = 1 (v/v). [f]The results were repeated at least twice. [g]Not determined.

As illustrated in Table 2, the phenylene content was determined as 4.99, 4.88, and 3.33 mmol/g for PMOs-B10T0-SH, HHBs-B8T2-SH, and HHBs-B5T5-SH. The SH content is similar for each sample, ranging from 0.40 to 0.45 mmol/g. Combined with the $^{29}Si$ MAS NMR data, the phenyl/OH molar ratio was estimated to gradually reduce for PMOs-B10T0-SH, HHBs-B8T2-SH, HHBs-B5T5-SH, and MCM-B0T10-SH, confirming the gradually increased hydrophilic surface. MCM-B0T10-SH exhibits a typical of type IV vapor adsorption isotherm with a C value in the BET equation of 5.07, displaying distinct hydrophilic surface (Table 2). PMOs-B10T0-SH gives a vapor adsorption isotherm of type V with a


dx.doi.org/10.1021/cs500385s | ACS Catal. 2014, 4, 2566−2576

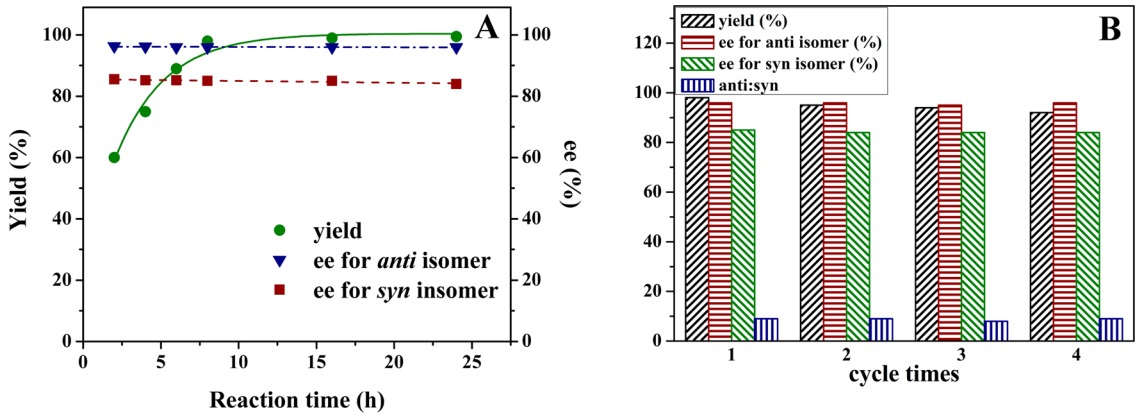


**Figure 4.** Variation of yield and ee of product catalyzed by HHBs-B8T2-Pro in the direct asymmetric aldol reaction of cyclohexanone with aldehydes in brine with (A) reaction time and (B) recycling runs.

*C* value of 0.83, characteristic of a hydrophobic surface. For HHBs-B8T2-SH, the vapor adsorption isotherm was observed as type V, similar to the shape observed for hydrophobic PMOs-B10T0-SH, although the *C* value was calculated to be 1.34. That is, HHBs-B8T2-SH is more hydrophilic than PMOs-B10T0-SH but more hydrophobic than MCM-B0T10-SH. Taking its pore wall structure into account, HHBs-B8T2-SH can be considered to have an alternating hydrophobic and hydrophilic surface. In addition, the wall thickness could be related with the hydrophobic−hydrophilic nature of mercaptopropyl-functionalized samples. Along with increasing hydrophilic properties, the wall thickness presents a slight increase. MCM-B0T10-SH exhibits a maximum wall thickness of 1.18 nm (Table 2).

After grafting *trans*-4-hydroxy-L-proline on the mesoporous support with hydrophobic (PMOs-B10T0-SH), alternating hydrophobic and hydrophilic (HHBs-B8T2-SH and HHBs-B5T5-SH), or hydrophilic (MCM-B0T10-SH) surface, as illustrated in Scheme 1, PMOs-B10T0-Pro (**2**), HHBs-B8T2-Pro (**3**), HHBs-B5T5-Pro (**4**), and MCM-B0T10-Pro (**5**) were produced. The FT-IR spectra of HHBs-B8T2-SH, HHBs-B8T2-Pro-BOC, and HHBs-B8T2-Pro confirm the grafting (Figure S6). The appearance of the adsorption bands at 2980 $cm^{-1}$ assigned to the $-CH_3$ of the L-proline, and the adsorption bands at 2920 and 2850 $cm^{-1}$ assigned to the $-CH_3$ of the BOC in the spectrum of HHBs-B8T2-Pro-BOC confirms the L-proline grafting. The disappearance of the adsorption bands for the $-CH_3$ of the BOC after the acid treatment proves the complete remove of the BOC groups. The covalent linkage of L-proline is further supported by the emerging signal at ca. 134.7 ppm assigned to phenylene in the $^{13}C$ CP/MAS NMR spectrum of MCM-B0T10-Pro, which was absent on MCM-B0T10-SH as the grafted precursor (Figure 3A). The N content in the resulting heterogeneous catalyst was calculated from element analysis as 0.34, 0.28, 0.25, and 0.23 mmol/g, which can be taken as the content of L-proline moiety in that the N quantity from template residue in mercaptopropyl-functionalized supports is detected as low as negligible, as shown in Table 2. It also indicates that S content was retained the same value after L-proline grafting (Table 2), revealing no Si−C bond hydrolysis occurred during the synthesis process. The grafting effectiveness for L-proline on PMOs-B10T0-SH, HHBs-B8T2-SH, HHBs-B5T5-SH, and MCM-B0T10-SH was calculated as 79%, 64%, 60% and 58% respectively, presenting a decrease with the increased hydrophilic surface property. TGA curves for HHBs-B8T2-SH and HHBs-B8T2-Pro are shown in Figure 3B. Compared with HHBs-B8T2-SH (37.1%), the weight loss (42.2%) from 400 to 800 °C for HHBs-B8T2-Pro not only included the decomposition of the organic species within the pore walls but also the decomposition of grafted L-proline. Thus, TGA results give an N content of L-proline of 0.30 mmol/g in HHBs-B8T2-Pro, showing a good accordance with the element analysis result of 0.28 mmol/g. In addition, after covalent grafting, the L-proline-grafted solids well preserve the ordered hexagonally symmetric mesoprous structures and the periodic structure, as can be seen from the XRD patterns (Figure 1b and Figure S1B) and TEM images (Figure S2, bottom images). The detailed textural properties of L-proline-grafted samples are given in Table 1. The textural structures hardly change with typical of type IV $N_2$ isotherms and narrowly distributed pore sizes are well retained (Figure S2B). The specific area and the pore volume of the L-proline-grafted samples remarkably reduce, better evidencing the covalent grafting (Table 1). As illustrated in Table 2, *C* values from the vapor adsorption measurements were estimated as 0.65, 1.24, 2.07, and 4.88 for PMOs-B10T0-Pro, HHBs-B8T2-Pro, HHBs-B5T5-Pro, and MCM-B0T10-Pro, confirming the gradually increased hydrophilic surface after L-proline grafting, despite that a slight decrease was observed for each samples compared with the mercaptopropyl-functionalized precursors.

**Catalytic Properties of Heterogeneous L-Proline-Grafted Mesoporous Silica and Catalyst Reusability.** The catalytic direct asymmetric aldol reaction was performed first with *p*-nitrobenzaldehyde and cyclohexanone as catalyzed substrates. As shown in Table 3, in either neat or aqueous medium (entries 1−21), all the heterogeneous catalysts prepared in this work, except MCM-B0T10-Pro in neat, are able to catalyze the aldol reaction of *p*-nitrobenzaldehyde and cyclohexanone that hardly occurred on homogeneous vinylbenzene-modified 4-OH-L-proline (**1**). In the neat environment (entries 1−5), PMOs-B10T0-Pro (**2**) gave a 58% yield (a TON of 7.0) in 24 h, affording 73% ee for *anti* isomer and 57% ee for *syn* isomer. HHBs-B8T2-Pro (**3**) gave similar TON value (6.4) to PMOs-B10T0-Pro (**2**) in the same reaction time, affording 42% yield in 24 h, 89% ee for *anti* isomer and 78% ee for *syn* isomer. HHBs-B5T5-Pro (**4**) gave 27% yield (a TON of 3.3) in 24 h with 80% ee for *anti* isomer and 60% ee for *syn* isomer. No reaction observed on the distinct hydrophilic MCM-B0T10-Pro (**5**). The ee observed with HHBs-B8T2-Pro (**3**) is comparable


dx.doi.org/10.1021/cs500385s | *ACS Catal.* 2014, 4, 2566−2576

to the observation in the homogeneous catalysis of L-proline in DMSO[31] but with a much lower proline loading.

The catalytic reaction was then performed in water (entries 7−12). PMOs-B10T0-Pro (**2**) gave 96% yield (a TON of 11.7) in 24 h, affording 22% ee for *anti* isomer and 14% ee for *syn* isomer. HHBs-B8T2-Pro (**3**) gave 83% yield (a TON of 12.6) in 24 h, affording 72% ee for *anti* isomer and 28% ee for *syn* isomer. Prolonging the reaction time from 24 to 48 h, the yield increases to 98% without expense of enantioselectivity. HHBs-B5T5-Pro (**4**) gave 48% yield (a TON of 5.7) in 24 h with 74% ee for *anti* isomer and 18% ee for *syn* isomer. On MCM-B0T10-Pro (**5**), 18% yield (a TON of 3.7) in 24 h, 25% ee for *anti* isomer and 6% ee for *syn* isomer were afforded.

In brine (entries 13−20), both yield and ee on PMOs-B10T0-Pro (2) were improved. A 62% yield was afforded in 8 h with 83% ee for anti isomer and 62% ee for *syn* isomer. When we prolonged the reaction time to 24 h, 99% yield was achieved, but the ee reduced to 72% ee for *anti* isomer and 39% ee for *syn* isomer. With HHBs-B8T2-Pro (**3**), the catalytic reaction was accomplished in 8 h, affording a yield of 98% and a TON of 14.9, and 96% ee for *anti* isomer and 85% ee for *syn* isomer (entry 16). Variation of yield and ee of product catalyzed by HHBs-B8T2-Pro in the direct asymmetric aldol reaction of cyclohexanone with aldehydes in brine with reaction time has been investigated, as shown in Figure 4A. Along with increasing reaction time, the yield exhibits a Langmuir type increase and the ee value holds at the same value during 24 h. This catalytic efficiency is even better than that observed for the catalysis of *trans*-4-(4-*tert*-butylphenoxy)-L-proline[41] or long-chain diamine derived proline with trifluoroacetic acid,[39] and the ee values are comparable to that observed in aqueous medium for the catalysis of *trans*-4-(4-*tert*-butylphenoxy)-L-proline[41] or long-chain diamine derived proline with trifluoroacetic acid[39] or siloxyproline.[38] On HHBs-B5T5-Pro (**4**), 31% yield was afforded in 24 h with 84% ee for *anti* isomer and 41% ee for *syn* isomer. MCM-B0T10-Pro (**5**) gave moderate yield and ee, similar to the observation in water. A further study demonstrated that, with HHBs-B8T2-Pro (**3**), the molar ratio of cyclohexanone to *p*-nitrobenzaldehyde can be reduced to 1.5/1 without compromising the diastereo- and enantioselectivity (entry 20). A visible direct asymmetric aldol addition has even been achieved under a catalyst loading of as low as 0.63 mol %, giving 54% yield in 24 h and 95% ee for anti-isomers and 81% ee for *syn*-isomers in saturated brine.

In either neat or aqueous medium, HHBs-B8T2-Pro (**3**) provides better diastereoselectivity than other heterogeneous catalysts investigated in this work. It is visible that the catalytic activity and enantioselectivity rely on the surface properties of catalyst solids and reaction medium markedly. In neat environment, either yield or TON increases with rising surface hydrophobicity. But in aqueous medium, HHBs-B8T2-Pro (**3**) shows superior activity to PMOs-B10T0-Pro (**2**). In each case, PMOs-B10T0-Pro (**2**) and HHBs-B8T2-Pro (**3**) exhibit higher activity than MCM-B0T10-Pro (**5**). The superior activity of hydrophobic or hydrophobic and hydrophilic alternating catalyst to hydrophilic catalyst can simply be attributed to the synergistic effects of the hydrophobic blocks in their channels. In neat condition, the hydrophobic channels of **2** and **3** advanced the access of organic reactants to the catalytic sites, thereby accelerating the reaction. In aqueous medium, the mesoporous channels were able to allure from aqueous medium and subsequently constrain organic reactants, increasing the reactant population around the catalytic sites. The catalytic rate of PMOs-B10T0-Pro (**2**) and HHBs-B8T2-Pro (**3**) was promoted more significantly in saturated brine than in water. This is supposed to originate from the additional contribution of the oil−water interfaces in the channels of **2** and **3**. The oil−water interface was reported previously[41,64] to play a critical role in the reaction acceleration in aqueous medium. In saturated brine, the oil−water interface is much clearer than that in water, able to implement the interfacial synergy more efficiently. Owing to its hydrophobic and hydrophilic alternating surface, HHBs-B8T2-Pro (**3**) benefits more from the interface, demonstrating higher yield in brine than hydrophobic PMOs-B10T0-Pro (**2**). However, a rise of the hydrophilic blocks reduces the catalytic activity. HHBs-B5T5-Pro (**4**) afforded lower yield than HHBs-B8T2-Pro (**3**) in each case.

In neat or aqueous environment, HHBs-B8T2-Pro (**3**) and HHBs-B5T5-Pro (**4**), both with alternating hydrophobic and hydrophilic blocks in pore walls, were found to afford higher enantioselectivity than either hydrophobic catalyst (**2**) or hydrophilic catalyst (**5**). Especially in brine, the ee values on all heterogeneous catalysts with hydrophobic blocks were visibly improved in comparison to in neat or in water. The oil−water interface existing in HHBs-B8T2-Pro (**3**) facilitated achieving an ee of as high as 96% in >99% yield. As reported previously, the oil−water interface could not only accelerate the reaction but also change the enantioselectivity in either pristine or derived L-proline-catalyzed aldol reactions.[41] When L-proline is placed at the effective oil−water interface and the reaction occurs around this interface, good yield and high enantioselectivity could be achieved probably due to the hydrogen bonds of the free −OH group of the interfacial water with the reactants and transition state. In the case of hydrophilic catalyst (**5**), the effective oil−water interface is difficult to form around the active sites, leading to not only lower yield but also poor ee. In brine, the oil/water interfaces are better defined than in water. To further verify the above analysis of role of the oil−water interfaces, the reaction medium was tailored as toluene and DMSO (entries 22−25). In toluene, HHBs-B8T2-Pro (**3**) is inferior to PMOs-B10T0-Pro (**2**) in both yield and ee. In DMSO, yield and ee were improved but still inferior to that in neat or in brine (entries 25). But when brine was then introduced to fabricate the oil−water interfaces (entry 24), the yield and ee with HHBs-B8T2-Pro (**3**) was both improved.

HHBs-B8T2-Pro (**3**) has been extensively applied to the aldol reactions of *m*- or *o*-nitrobenzaldehydes with cyclohexanone that were reported as more difficult to be catalyzed by proline derivatives.[41,48] For the aldol reactions of *m*-nitrobenzaldehydes with cyclohexanone in brine (entry 26), 93% yield was afforded in 48 h with 75% ee for *anti* isomer. For the aldol reactions of *o*-nitrobenzaldehydes with cyclohexanone in brine (entry 27), 78% yield was afforded in 48 h with 92% ee for *anti* isomer. HHBs-B8T2-Pro (**3**) was then applied to the aldol reactions of ethyl-(2)-oxoacetate with cyclohexanone, which produces a key intermediate for the synthesis of statine and its analogues.[65] An 81% yield was afforded in 24 h with 90% ee for *anti* isomer (entry 28).

The catalyst reusability has also been investigated. The catalyst was easily separated from the reaction system by centrifugation and recycled well. All of the yield and enantiselectivity, as well as diastereoselectivity, hold at the same level in three runs, as shown in Figure 4. Almost no leaching was observed for HHBs-B8T2-Pro and HHBs-B5T5-Pro (<1%) after three runs, whereas 1.5% and 1.7% were

observed for PMOs-B10T0-Pro and MCM-B0T10-Pro (Table S1). The recycled catalysts in three runs have effectively preserved the long-range ordered mesoporous structures and the periodic structure (Figure S7).

The catalysis of HHBs-B8T2-Pro (**3**) was then evaluated with the Knoevenagel–Michael cascade reaction of isatin, malononitrile, and acetone with PMOs-B10T0-Pro (**2**), HHBs-B5T5-Pro (**4**) and MCM-B0T10-Pro (**5**) as control catalysts, as illustrated in Table 4. The Knoevenagel–Michael cascade reaction of isatin, malononitrile, and acetone is an effective approach to produce 3,3′-disubstituted oxindole which has triggered great synthetic interest.[59] To our delight, in THF/brine, PMOs-B10T0-Pro (**2**) afforded 90% yield and 93% ee, and HHBs-B8T2-Pro (**3**) afforded 85% yield and 91% ee (Table 4). In toluene/brine, PMOs-B10T0-Pro (**2**) afforded 55% yield and 82% ee, and HHBs-B8T2-Pro (**3**) afforded 64% yield and 91% ee. HHBs-B5T5-Pro (**4**) gave a similar variation with HHBs-B8T2-Pro (**3**), despite the lower yield and ee than HHBs-B8T2-Pro (**3**). In either THF/brine or toluene/brine, MCM-B0T10-Pro (**5**) gave inferior yield and ee to PMOs-B10T0-Pro (**2**), HHBs-B8T2-Pro (**3**), and HHBs-B5T5-Pro (**4**). In THF/brine which has no liquid–liquid oil–water interfaces, PMOs-B10T0-Pro (**2**) and HHBs-B8T2-Pro (**3**) gave similar yield and ee, although in toluene/brine, which has liquid–liquid oil–water interfaces, HHBs-B8T2-Pro (**3**) gave higher yield and better ee than PMOs-B10T0-Pro (**2**). The results further indicate that hydrophobic and hydrophilic alternating surface contributes to the heterogeneous catalysis. Variation of yield of product and intermediate and ee of product catalyzed by HHBs-B8T2-Pro in the Knoevenagel–Michael cascade reaction in toluene/brine with reaction time has been investigated, as shown in Figure 5A. Along with the reaction time, the yield of product exhibits an S-type curve, and the ee value presents a decrease of <2% toward the reaction time. The yield of the intermediate isatylidine malononitrile increases in the first 4 h and then slowly decreases to 9% at 10 h. It has been reported that the reaction rate for the Knoevenagel reaction is much faster than the following Michael reaction,[59] leading to an induction period for the whole cascade process. The yield and enantiselectivity hold at the same level in three runs, as shown in Figure 5B. Almost no leaching was also observed for HHBs-B8T2-Pro.

**Table 4. Knoevenagel–Michael Cascade Reaction of Isatin, Malononitrile, and Acetone**[a]

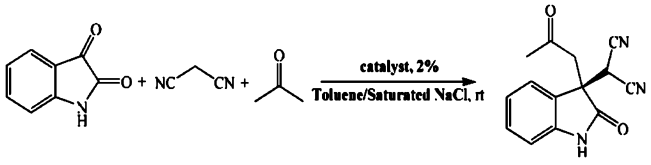


| entry | solvent | catalyst | proline loading (mol %) | TON | yield (%) | ee (%)[b] |
|---|---|---|---|---|---|---|
| 1 | THF/brine[c] | 1 | 20.0 | | | |
| 2 | THF/brine[c] | 2 | 15.0 | 6.1 | 90 | 93 |
| 3 | THF/brine[c] | 3 | 13.0 | 6.9 | 85 | 91 |
| 4 | THF/brine[c] | 4 | 12.0 | 5.6 | 78 | 86 |
| 5 | THF/brine[c] | 5 | 11.2 | 4.1 | 36 | 84 |
| 6 | toluene/brine[d] | 1 | 20.0 | | | |
| 7 | toluene/brine[d] | 2 | 15.0 | 4.3 | 55 | 82 |
| 8 | toluene/brine[d] | 3 | 13.0 | 5.4 | 64 | 91 |
| 9 | toluene/brine[d] | 4 | 12.0 | 4.4 | 57 | 84 |
| 10 | toluene/brine[d] | 5 | 11.2 | 3.2 | 26 | 63 |

[a]Conditions: isatin (0.5 mmol), malonitrile 0.5 mmol), acetone (0.5 mmol), and solvent (5 mL); reaction time: 10 h. [b]Determined by $^1$H NMR of the crude product and chiral-phase HPLC analysis (chiralcel AD-H). [c]THF/brine = 4/1 (v/v). [d]Toluene/brine = 1 (v/v). [e]The results were repeated at least twice.

**Possible Heterogeneous Catalytic Mechanism.** There is one common observation on each heterogeneous L-proline catalyst: a configuration inversion occurred. It was previously reported that the aldol reaction of cyclohexanone and *p*-nitrobenzaldehyde, catalyzed by either L-proline in DMSO[31] or L-proline derivatives in water or neat cyclohexanone,[38−41] generally afforded (2*S*, 1′*R*) isomer as the major product. But in our case, the (2*R*, 1′*S*) isomer was afforded as the major product. According to the mechanism reported previously,[30,31,66,67] in the proline-catalyzed homogeneous asymmetric aldol reaction, aldehyde served to attack the enamine of ketone. The transition states involving the *re*-attack on the *anti*-enamine (yield 2*S*, 1′*R* and 2*S*, 1′*S*) were lower in energy than the transition states for the *si*-attack on the *syn*-enamine (yield 2*R*, 1′*S* and 2*R*, 1′*R*), giving (2*S*, 1′*R*) isomer as the major product. But for the L-proline grafted on the mesoporous supports for PMOs-B10T0-Pro (**2**), HHBs-B8T2-Pro (**3**), HHBs-B5T5-Pro (**4**), and MCM-B0T10-Pro (**5**), the meso-

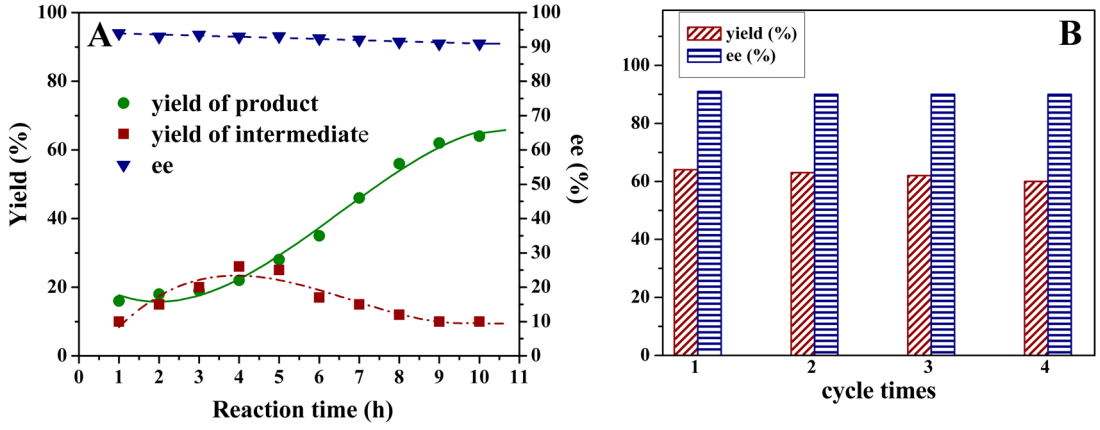


**Figure 5.** Variation of yield of product and intermediate and ee of product catalyzed by HHBs-B8T2-Pro in the Knoevenagel–Michael cascade reaction in toluene/brine with (A) reaction time and (B) recycling runs.


dx.doi.org/10.1021/cs500385s | *ACS Catal.* 2014, 4, 2566−2576

Scheme 2. Mesoporous Channels Obstruct the *re*-attack of Aldehyde on *Anti*-Enamine of Ketone in the Channels of (a) PHHBs, (b) PMOs, and (c) MCM Materials

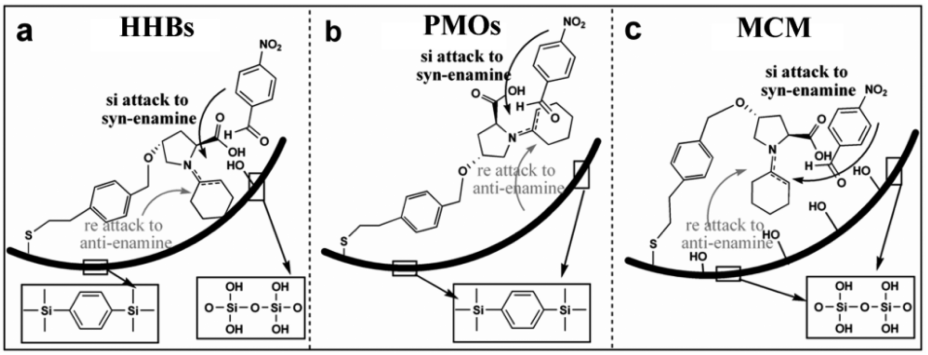


Scheme 3. Cyclohexanone–Water Interfaces in the Channels of (a) PHHBs-B8T2-Pro (3) and (b) PMOs-B10T0-Pro (2)

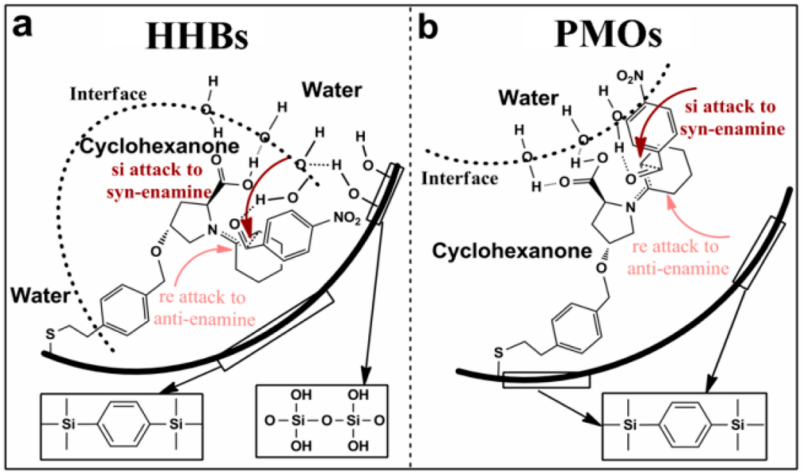


porous channels could all hinder the *re*-attack on *anti*-enamine, leading to the inverse configuration, as illustrated in Scheme 2. In the neat environment, HHBs-B8T2-Pro (**3**) had more powerful confinement than PMOs-B10T0-Pro (**2**) or MCM-B0T10-Pro (**5**) because the carboxylic group of L-proline in HHBs-B8T2-Pro (**3**) prefers to orientate close to the hydrophilic blocks, although the benzene ring of the linker prefers to locate close to the hydrophobic part of the pore walls (Scheme 2).

To further confirm the synergetic effect between hydrophobic and hydrophilic structural counterparts, the passivation of −OH groups of HHBs-B8T2-Pro (HHBs-B8T2-Pro-$CH_3$) was performed. HHBs-B8T2-Pro-$CH_3$ was applied to the direct asymmetric aldol reaction of *p*-nitrobenzaldehyde and cyclohexanone. In neat, HHBs-B8T2-Pro-$CH_3$ (**3′**) gave a TON value of 6.0 (41% yield) in 24 h, and 78% ee for *anti* isomer and 56% ee for *syn* isomer (Table 3, entry 6). The passivation of −OH groups had essentially no adverse effects on the activity but resulted in slightly lower enantioselectivity. In brine, HHBs-B8T2-Pro-$CH_3$ (**3′**) gave a TON value of 11.3 in 24 h (85% yield), and 80% ee or *anti* isomer and 20% ee for *syn* isomer (Table 3, entry 21). The passivation of −OH groups caused a decrease in both yield and ee. It supports the viewpoints that the acceleration of the reaction depends on the hydrophobic channels in the neat condition while relying on the oil–water interface in brine, and the enantioselectivity promotion depends on the oil–water interface both in neat and brine. The enhancement of ee in saturated brine, achieved on HHBs-B8T2-Pro (**3**) and PMOs-B10T0-Pro (**2**), is supposed to result from the effective interfaces created in the nanochannels. The pore wall of L-proline-grafted PMOs and HHBs materials provided the hydrophobic environment and thus formed the effective oil–water interface, like the hydrophobic pocket when aldolase enzymes catalyze the reaction in water.[68] As reported previously,[41,69] oil–water interface could not only accelerate reaction but also change enantioselectivity in either pristine or derived L-proline-catalyzed aldol reactions. The oil–water interface is envisioned to play a crucial role in diminishing the contacts between bulk water and the reaction transition states. Moreover, the reaction is supposed to be facilitated by the hydrogen bonding at the oil-in-water interface. Although the oil–water interfaces could be formed in the channels of both HHBs-B8T2-Pro (**3**) and PMOs-B10T0-Pro (**2**), their interfacial shapes are different, resulting in a difference in the ee improvement, as proposed in Scheme 3. In the channels of HHBs-B8T2-Pro (**3**), the hydrophobic and hydrophilic alternating surface leads to intermittent convex oil–water interfaces around the catalytic sites. The convex interfaces have no any adverse effect on the confinement. In the channels of PMOs-B10T0-Pro (**2**), however, the organic reactants are located along the hydrophobic pore wall and water at the center regions of the channels, forming a concave continuous interface.

As proposed in Scheme 3, when the aldol reaction occurs at oil–water interfaces, the stability of transition states for (2*R*, 1′*S*) and (2*S*, 1′*S*) are increased due to the hydrogen bonding


dx.doi.org/10.1021/cs500385s | *ACS Catal.* 2014, 4, 2566–2576

between $H_2O$ with aldehyde, thereby promoting the ee of the isomers. However, in pure water, the oil/water interfaces are poorer defined, producing cyclohexanone−water miscible zones around the carboxylic group of L-proline. The miscible zones are supposed to decrease the stability of the transition states for (2*R*, 1′*S*) and (2*S*, 1′*S*) due to the interaction of the phenyl ring with water.

## CONCLUSION

In summary, we have developed a highly efficient heterogeneous asymmetric catalyst with alternating hydrophobic and hydrophilic blocks in its pore wall, which demonstrates surface synergies in the neat environment and interface acceleration in aqueous medium, thereby promoting catalytic rate and enantioselectivity impressively in the direct aldol reaction and Knoevenagel−Michael cascade reaction. Further studies focusing on the modulation of hydrophobic and hydrophilic period of the support and the corresponding impact to the catalysis in more exigent reaction are currently under investigation and will be reported in due course.

## ASSOCIATED CONTENT

### Supporting Information

XRD patterns, TEM images, $N_2$ adsorption−desorption isotherms, $^{13}C$ CP/MAS NMR spectra, vacuum FT-IR spectra, $^1H$ NMR data, and HPLC data of the products. This material is available free of charge via the Internet at http://pubs.acs.org.

## AUTHOR INFORMATION

### Corresponding Author

*E-mail: hejing@mail.buct.edu.cn. Fax: +86-10-6442 5385 . Tel.: +86-10-6442 5280.

### Notes

The authors declare no competing financial interest.

## ACKNOWLEDGMENTS

This work is supported by NSFC, PCSIRT (IRT1205), and 973 Project (2011CBA00504). J.H. particularly appreciates the financial aid of China National Funds for Distinguished Young Scientists from the NSFC.

## REFERENCES

(1) Tanev, P. T.; Chibwe, M.; Pinnavaia, T. J. *Nature* **1994**, *368*, 321−323.
(2) Margelefsky, E. L.; Zeidanb, R. K.; Davis, M. E. *Chem. Soc. Rev.* **2008**, *37*, 1118−1126.
(3) Motokura, K.; Tada, M.; Iwasawa, Y. *J. Am. Chem. Soc.* **2007**, *129*, 9540−9541.
(4) Motokura, K.; Tada, M.; Iwasawa, Y. *Angew. Chem., Int. Ed.* **2008**, *47*, 9230−9235.
(5) Motokura, K.; Tada, M.; Iwasawa, Y. *J. Am. Chem. Soc.* **2009**, *131*, 7944−7945.
(6) Trindade, A. F.; Gois, P. M. P; Afonso, C. A. M. *Chem. Rev.* **2009**, *109*, 418−514.
(7) Xiang, S.; Zhang, Y. L.; Xin, Q.; Li, C. *Angew. Chem., Int. Ed.* **2002**, *41*, 821−824.
(8) Yang, H. Q.; Li, J.; Yang, J.; Liu, Z. M.; Yang, Q. H.; Li, C. *Chem. Commun.* **2007**, 1086−1088.
(9) Wan, Y.; Zhao, D. Y. *Chem. Rev.* **2007**, *107*, 2821−2860.
(10) Hoffmann, F.; Cornelius, M.; Morell, J.; Fröba, M. *Angew. Chem., Int. Ed.* **2006**, *45*, 3216−3251.
(11) Li, C.; Zhang, H. D.; Jiang, D. M.; Yang, Q. H. *Chem. Commun.* **2007**, 547−558.
(12) Yang, Q. H.; Han, D. F.; Yang, H. Q.; Li, C. *Chem.—Asian J.* **2008**, *3*, 1214−1229.
(13) Yu, C.; He, J. *Chem. Commun.* **2012**, *48*, 4933−4940.
(14) Yang, H. Q.; Zhang, L.; Zhong, L.; Yang, Q. H.; Li, C. *Angew. Chem., Int. Ed.* **2007**, *46*, 6861−6865.
(15) Jones, M. D.; Raja, R.; Thomas, J. M.; Johnson, B. F. G.; Lewis, D. W.; Rouzaud, J.; Harris, K. D. M. *Angew. Chem., Int. Ed.* **2003**, *42*, 4326−4331.
(16) Raja, R.; Thomas, J. M.; Jones, M. D.; Johnson, B. F. G.; Vaughan, D. E. W. *J. Am. Chem. Soc.* **2003**, *125*, 14982−14983.
(17) Hsiao, L. H.; Chen, S. Y.; Huang, S. J.; Liu, S. B.; Chen, P. H.; Chan, J. C.; Cheng, S. *Appl. Catal., A* **2009**, *359*, 96−107.
(18) Bae, S. J.; Kim, S. W.; Hyeon, T.; Kim, B. M. *Chem. Commun.* **2000**, 31−32.
(19) Dalko, P. I.; Moisan, L. *Angew. Chem., Int. Ed.* **2001**, *40*, 3726−3748.
(20) Dondoni, A.; Massi, A. *Angew. Chem., Int. Ed.* **2008**, *47*, 4638−4660.
(21) Eder, U.; Sauer, G.; Wiechert, R. *Angew. Chem., Int. Ed.* **1971**, *10*, 496−497.
(22) Hajos, Z. G.; Parrish, D. R. *J. Org. Chem.* **1974**, *39*, 1615−1621.
(23) List, B. *Tetrahedron.* **2002**, *58*, 5573−5590.
(24) List, B. *Acc. Chem. Res.* **2004**, *37*, 548−557.
(25) Notz, W.; Tanaka, F.; Barbas, C. F., III. *Acc. Chem. Res.* **2004**, *37*, 580−591.
(26) List, B. *J. Am. Chem. Soc.* **2000**, *122*, 9336−9337.
(27) List, B.; Pojarliev, P.; Biller, W. T.; Martin, H. J. *J. Am. Chem. Soc.* **2002**, *124*, 827−833.
(28) List, B.; Pojarliev, P.; Martin, H. *J. Org. Lett.* **2001**, *3*, 2423−2425.
(29) Kumaragurubaran, N.; Juhl, K.; Zhuang, W.; Bøgevig, A.; Jørgensen, K. A. *J. Am. Chem. Soc.* **2002**, *124*, 6254−6255.
(30) List, B.; Lerner, R. A.; Barbas, C. F., III. *J. Am. Chem. Soc.* **2000**, *122*, 2395−2396.
(31) Sakthivel, K.; Notz, W.; Bui, T.; Barbas, C. F., III. *J. Am. Chem. Soc.* **2001**, *123*, 5260−5267.
(32) Notz, W.; List, B. *J. Am. Chem. Soc.* **2000**, *122*, 7386−7387.
(33) Northrup, A. B.; MacMillan, D. W. C. *J. Am. Chem. Soc.* **2002**, *124*, 6798−6799.
(34) Northrup, A. B.; Mangion, I. K.; Hettche, F.; MacMillan, D. W. C. *Angew. Chem., Int. Ed.* **2004**, *43*, 2152−2154.
(35) Pidathala, C.; Hoang, L.; Vignola, N.; List, B. *Angew. Chem., Int. Ed.* **2003**, *42*, 2785−2788.
(36) Tang, Z.; Yang, Z. H.; Chen, X. H.; Cun, L. F.; Mi, A. Q.; Jiang, Y. Z.; Gong, L. Z. *J. Am. Chem. Soc.* **2005**, *127*, 9285−9289.
(37) Tang, Z.; Jiang, F.; Yu, L. T.; Cui, X.; Gong, L. Z.; Mi, A. Q.; Jiang, Y. Z.; Wu, Y. D. *J. Am. Chem. Soc.* **2003**, *125*, 5262−5263.
(38) Hayashi, Y.; Sumiya, T.; Takahashi, J.; Gotoh, H.; Urushima, T.; Shoji, M. *Angew. Chem., Int. Ed.* **2006**, *45*, 958−961.
(39) Mase, N.; Nakai, Y.; Ohara, N.; Yoda, H.; Takabe, K.; Tanaka, F.; Barbas, C. F., III. *J. Am. Chem. Soc.* **2006**, *128*, 734−735.
(40) Hayashi, Y.; Aratake, S.; Okano, T.; Takahashi, J.; Sumiya, T.; Shoji, M. *Angew. Chem., Int. Ed.* **2006**, *45*, 5527−5529.
(41) Huang, J.; Zhang, X.; Armstrong, D. W. *Angew. Chem.* **2007**, *119*, 9231−9235.
(42) Gruttadauria, M.; Giacalone, F.; Marculescu, A. M.; Meo, P. L.; Riela, S.; Noto, R. *Eur. J. Org. Chem.* **2007**, *28*, 4688−4698.
(43) Gruttadauria, M.; Giacalone, F.; Noto, R. *Adv. Synth. Catal.* **2009**, *351*, 33−57.
(44) Doyagüez, E. G.; Calderón, F.; Sánchez, F.; Fernández-Mayoralas, A. *J. Org. Chem.* **2007**, *72*, 9353−9356.
(45) Gao, J. S.; Liu, J.; Jiang, D. M.; Xiao, B.; Yang, Q. H. *J. Mol. Catal. A: Chem.* **2009**, *313*, 79−87.
(46) Zamboulis, A.; Rahier, N. J.; Gehringer, M.; Cattoën, X.; Niel, G.; Bied, C.; Moreau, J. J. E.; Man, M. W. C. *Tetrahedron: Asymmetry* **2009**, *20*, 2880−2885.
(47) An, Z.; Zhang, W. H.; Shi, H. M.; He, J. *J. Catal.* **2006**, *241*, 319−327.

(48) Gao, J. S.; Liu, J.; Tang, J. T.; Jiang, D. M.; Li, B.; Yang, Q. H. *Chem.—Eur. J.* **2010**, *16*, 7852−7858.
(49) Jebors, S.; Enjalbal, C.; Amblard, M.; Mehdi, A.; Subra, G.; Martinez, J. *J. Mater. Chem.* **2013**, *1*, 2921−2925.
(50) Giacalone, F.; Gruttadauria, M.; Marculescu, A. M.; Noto, R. *Tetrahedron Lett.* **2007**, *48*, 255−259.
(51) Gruttadauria, M.; Giacalone, F.; Marculescu, A. M.; Salvo, A. M. P.; Noto, R. *ARKIVOC* **2009**, *8*, 5−15.
(52) Gruttadauria, M.; Giacalone, F.; Marculescu, A. M.; Noto, R. *Adv. Synth. Catal.* **2008**, *350*, 1397−1405.
(53) Gruttadauria, M.; Salvo, A. M. P.; Giacalone, F.; Agrigento, P.; Noto, R. *Eur. J. Org. Chem.* **2009**, *31*, 5437−5444.
(54) Giacalone, F.; Gruttadauria, M.; Agrigento, P.; Campisciano, V.; Noto, R. *Catal. Commun.* **2011**, *16*, 75−80.
(55) Yang, Q. H.; Kapoor, M. P.; Inagaki, S. *J. Am. Chem. Soc.* **2002**, *124*, 9694−9695.
(56) Zhao, X. S.; Audsley, F.; Lu, G. Q. *J. Phys. Chem. B* **1998**, *102*, 4143−4146.
(57) Kruk, M.; Jaroniec, M.; Sayari, A. *Langmuir* **1997**, *13*, 6267−6273.
(58) Pousse, G.; Cavelier, F. L.; Humphreys, L.; Rouden, J.; Blanchet. *J. Org. Lett.* **2010**, *12*, 3582−3585.
(59) Liu, L.; Wu, D.; Li, X.; Wang, S.; Li, H.; Li, J.; Wang, W. *Chem. Commun.* **2012**, *48*, 1692−1694.
(60) Inagaki, S.; Guan, S. Y.; Ohsuna, T.; Terasaki, O. *Nature* **2002**, *416*, 304−307.
(61) García, N.; Benito, E.; Guzmán, J.; Tiemblo, P.; Morales, V.; García, R. A. *Microporous Mesoporous Mater.* **2007**, *106*, 129−139.
(62) Kapoor, M. P.; Setoyama, N.; Yang, Q.; Ohashi, M.; Inagaki, S. *Langmuir* **2005**, *21*, 443−449.
(63) Yang, Q.; Kapoor, M. P.; Shirokura, N.; Ohashi, M.; Inagaki, S.; Kondoc, J. N.; Domen, K. *J. Mater. Chem.* **2005**, *15*, 666−673.
(64) Jung, Y.; Marcus, R. A. *J. Am. Chem. Soc.* **2007**, *129*, 5492−5502.
(65) Tao, J.; Hoffman, R. V. *J. Org. Chem.* **1997**, *62*, 6240−6244.
(66) Bahmanyar, S.; Houk, K. N.; Martin, H. J.; List, B. *J. Am. Chem. Soc.* **2003**, *125*, 2475−2479.
(67) Hoang, L.; Bahmanyar, S.; Houk, K. N.; List, B. *J. Am. Chem. Soc.* **2003**, *125*, 16−17.
(68) Berkssel, A.; Groger, H. *Asymmetric Organocatalysis*; Wiley-VCH: Weinheim, 2005.
(69) Delaney, J. P.; Brozinski, H. L.; Henderson, L. C. *Org. Biomol. Chem.* **2013**, *11*, 2951−2960.